Available online at www.sciencedirect.com
SCIENCE DIRECT®
Journal of Sound and Vibration 271 (2004) 599–614
JOURNAL OF SOUND AND VIBRATION
www.elsevier.com/locate/jsvi

The multi-body system modelling of the Gough–Stewart platform for vibration control

Yuan Cheng*, Gexue Ren, ShiLiang Dai

Department of Engineering Mechanics, Tsinghua University, Beijing 100084, China

Received 1 August 2002; accepted 10 March 2003

Abstract

This paper studies the dynamics and control of the Gough–Stewart platform for vibration control of a flexible supporting structure. The problem arises from a large radio telescope in which the astronomical equipment is mounted on a platform to be stabilized by a Gough–Stewart platform, while the base platform of the mechanism itself is carried by a vibrating cable-car that moves along flexible cables. As the base platform is not fixed on the ground, the reaction force caused by the motion of the stabilized platform will lead to perturbation on the base platform, and will induce vibration of the whole system. To study the feasibility for vibration control, this paper models the Stewart parallel mechanism as a multi-body systems with an elastically restrained base platform by the Newton–Euler method and proposes a PD control law based on the position prediction of the two platforms. Control simulations are carried out with the simulated wind excitations. The control effects are evaluated by comparing the root-mean-square responses of the stabilized platform.

1. Introduction

The Gough–Stewart platform [1] has the capability to control the six degrees of freedom of its payload platform, and has been proven to be of high positioning accuracy while maintaining high force-to-weight ratio. So, it is chosen to stabilize the receivers of a 500 m-aperture radio telescope [2], which has a spherical focal surface with an aperture of 250 m and the focal surface is 150 m above the reflector. To observe 5 GHz radio waves, the astronomical receivers are required to follow tracks on the focal surface with 4 mm positioning precision. In the platformless-feed-support concepts [3,4], the receivers are either driven by cables or carried by a cable car. The

*Corresponding author. fax: +86-10-6278-1824.
E-mail address: ycheng99@mails.tsinghua.edu.cn (Y. Cheng).

0022-460X/03/$ - see front matter © 2003 Elsevier Ltd. All rights reserved.
doi:10.1016/S0022-460X(03)00283-9

expected wind-induced vibration might be as high as 0.5 m, much higher than the specifications. The Gough–Stewart platform in this application has two movable platforms connected by six extensible legs. One of the platforms is the stabilized platform, on which the astronomical receivers are fixed, the other is the base platform that is mounted on the cable car. The objective is to alleviate the vibration of the stabilized platform by adjusting the six actuators on the legs with appropriate control laws when the base platform vibrates with the wind-induced cable car.

There are many publications on the dynamics and control of the Gough–Stewart platform [5–9], but in most of these works, the base platform is fixed. Studies [10,11] have investigated the use of Gough–Stewart platform for vibration isolation, but they are concentrated on vibrations of small amplitude and as the inertia of the base is much higher than that of the payload, the couple effect of the two platforms is not prominent.

In the application presented in this paper, the two platforms are dynamically coupled. The reaction force caused by the motion of the stabilized platform will lead to perturbation on the base platform, and will induce vibration of the whole system. This paper models the Gough–Stewart parallel mechanism as a multi-body system with a flexible supported base platform and proposes a PD control law based on the position prediction of the two platforms. Firstly, the Gough–Stewart platform for active vibration reduction is briefly introduced and the system is described as a standard control system. Then, the rigid multi-body modelling of the system is carried out in terms of the Newton–Euler equations. Finally, a PD control law is proposed and the control effects are simulated under the generated wind excitations. Conclusions regarding the feasibility of the Gough–Stewart platform for active vibration reduction are tentatively drawn.

2. The description of the plant

The model of the radio telescope is shown in Fig. 1. As shown in Fig. 2, the flexible supporting structure (including 8 suspension load cables and 4 pretension stabilized cables) supports the base platform (including the cable car in the Fig. 1) of the Gough–Stewart platform. The two platforms are connected by six extensible legs with spherical joints at the stabilized platform end and universal joints at the base platform end. The payloads are installed on the stabilized platform.

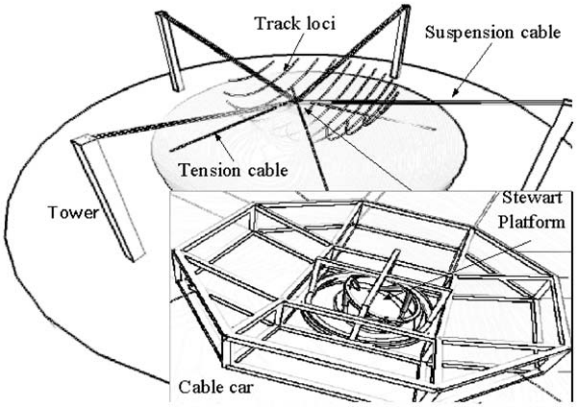

Fig. 1. Support structure of the radio telescope.

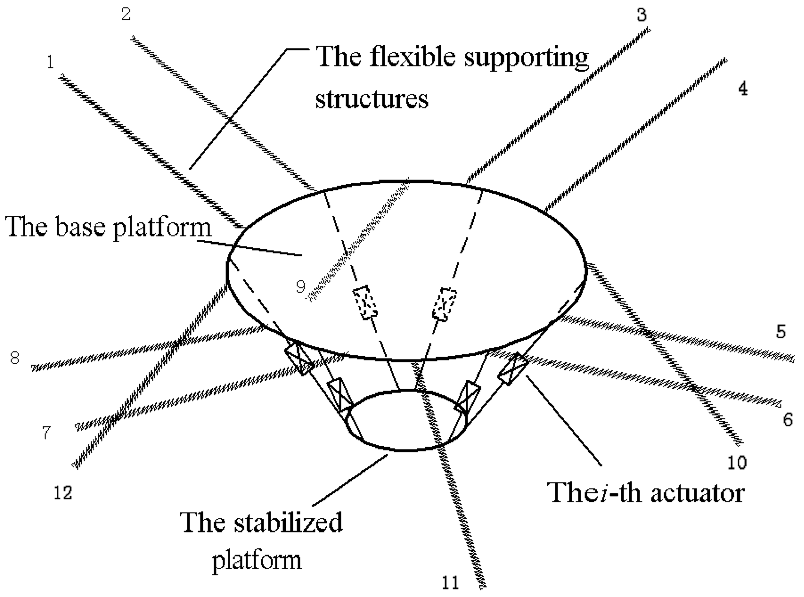

Fig. 2. Working diagram of the flexible supported Stewart platform. 1–8: suspension cables; 9–12: pretension stabilized cables.

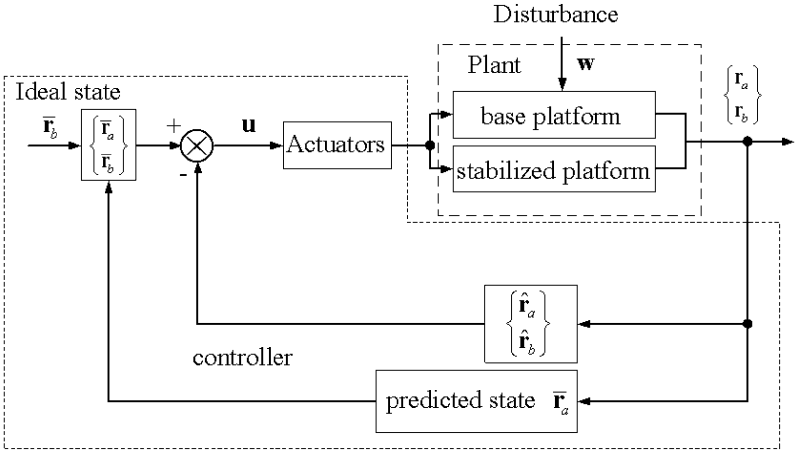

Fig. 3. Schematic representation of the control system.

The objective is to alleviate the vibration of the stabilized platform by adjusting the six actuators when the base platform is disturbed by winds or other unknown excitations. The controlled variables of the system are displacements of the stabilized platform and the controls are the strokes of the six actuators on the legs. Assuming the position of the two platforms can be observed, the control system can be illustrated by Fig. 3: through observing the responses of the base platform $\hat{\mathbf{r}}_a$ and the stabilized platform $\hat{\mathbf{r}}_b$, predict the position vector $\bar{\mathbf{r}}_a$ of the base platform and find the appropriate control $\mathbf{u}(t)$, i.e., strokes for the six actuators so that the displacement

$\mathbf{x}_b = \hat{\mathbf{r}}_b - \bar{\mathbf{r}}_b$ of the stabilized platform from its ideal position $\bar{\mathbf{r}}_b$ is under the given root-mean-square specification

$$\sqrt{E[x_{bi}(t)x_{bi}(t)]} \leqslant \delta_i, \tag{1}$$

where $i = 1, 2, \ldots, 6$ indicate the six components of $\mathbf{x}_b$. In Fig. 3, the top operator "$\wedge$" gives observed state, and "$-$" gives predicated valuable or ideal position.

3. The governing equations of the plant

In this section, the dynamic modelling of the multi-body system of the plant is carried out in terms of the Newton–Euler equations with Lagrange multipliers.

3.1. The governing equations of the plant

The multi-body dynamics model of the Gough–Stewart platform mechanism shown in Fig. 2 includes 14 rigid bodies. Two of which represent the base and stabilized platforms, and every leg is composed of two rigid bodies. Fig. 4 illustrates the base platform, stabilized platform and the ith leg of the Gough–Stewart platform. In the following equations, the subscript "a" denotes the base platform, "b" denotes the stabilized platform, "Ui" denotes the upper part of the ith leg and "Li" denotes the low part of the ith leg ($i = 1, 2, \ldots, 6$). Let $X'_k Y'_k Z'_k$ be the corresponding local reference frame, let $\mathbf{r}_k$ denote the position vector of center of mass of body k, and $\mathbf{p}_k$ be the Euler parameter orientation co-ordinates of the kth rigid body with reference to the global reference frame XYZ. Let $\mathbf{s}'_{ai}$ and $\mathbf{s}'_{bi}$, respectively, denote the position vector of point P_{ai} in the frame $X'_a Y'_a Z'_a$, and that of point P_{bi} in $X'_b Y'_b Z'_b$.

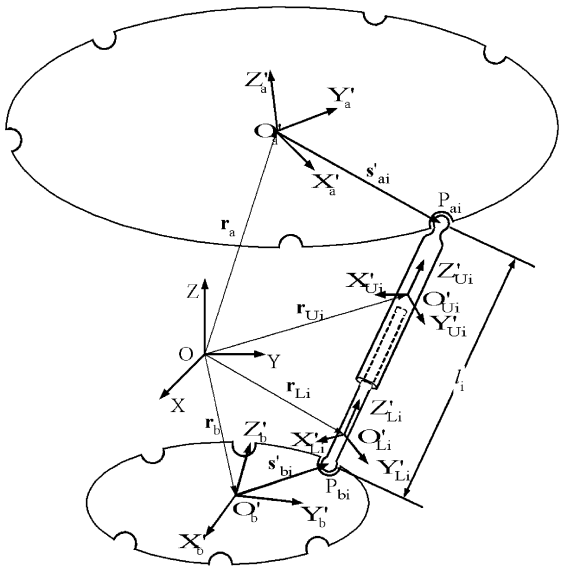

Fig. 4. Diagrammatic representation of connecting the two platforms.

To further simplify the notation, define

$$\begin{aligned}
&\mathbf{r} = \left[\mathbf{r}_a^{\mathrm{T}}, \mathbf{r}_b^{\mathrm{T}}, \mathbf{r}_{U1}^{\mathrm{T}}, \mathbf{r}_{L1}^{\mathrm{T}}, \ldots, \mathbf{r}_{U6}^{\mathrm{T}}, \mathbf{r}_{L6}^{\mathrm{T}}\right],\\
&\mathbf{p} = \left[\mathbf{p}_a^{\mathrm{T}}, \mathbf{p}_b^{\mathrm{T}}, \mathbf{p}_{U1}^{\mathrm{T}}, \mathbf{p}_{L1}^{\mathrm{T}}, \ldots, \mathbf{p}_{U6}^{\mathrm{T}}, \mathbf{p}_{L6}^{\mathrm{T}}\right],\\
&\mathbf{G} = \mathrm{diag}\,(\mathbf{G}_a, \mathbf{G}_b, \mathbf{G}_{U1}, \mathbf{G}_{L1}, \ldots, \mathbf{G}_{U6}, \mathbf{G}_{L6}),\\
&\mathbf{M} = \mathrm{diag}\,(m_a\mathbf{I}_3, m_b\mathbf{I}_3, m_{U1}\mathbf{I}_3, m_{L1}\mathbf{I}_3, \ldots, m_{U6}\mathbf{I}_3, m_{L6}\mathbf{I}_3),\\
&\mathbf{J}' = \mathrm{diag}(\mathbf{J}'_a, \mathbf{J}'_b, \mathbf{J}'_{U1}, \mathbf{J}'_{L1}, \ldots, \mathbf{J}'_{U6}, \mathbf{J}'_{L6}),\\
&\mathbf{F}^A = \left[\mathbf{F}_a^{A\mathrm{T}}, \mathbf{F}_b^{A\mathrm{T}}, \mathbf{F}_{U1}^{A\mathrm{T}}, \mathbf{F}_{L1}^{A\mathrm{T}}, \ldots, \mathbf{F}_{U6}^{A\mathrm{T}}, \mathbf{F}_{L6}^{A\mathrm{T}}\right],\\
&\mathbf{n}'^A = \left[\mathbf{n}_a'^{A\mathrm{T}}, \mathbf{n}_b'^{A\mathrm{T}}, \mathbf{n}_{U1}'^{A\mathrm{T}}, \mathbf{n}_{L1}'^{A\mathrm{T}}, \ldots, \mathbf{n}_{U6}'^{A\mathrm{T}}, \mathbf{n}_{L6}'^{A\mathrm{T}}\right].
\end{aligned} \tag{2}$$

where m_k is the mass of the kth body. $\mathbf{F}_k^A$ and $\mathbf{n}_k'^A$ are the force and torque acting on the kth body, including applied force and torque as well as and constraint force and torque. $\mathbf{J}'_k$ is the moment of inertia with respect to the origin of the centroidal reference frame of the ith body. The 3×4 matrix $\mathbf{G}_k$ is defined in Eq. (A.5) (Appendix A) and $\mathbf{I}_3$ is the 3×3 identity matrix.

The Newton–Euler formulation with Lagrange multipliers of the governing equations of the Euler parameters of the system is given by [12]

$$\begin{bmatrix} \mathbf{M} & \mathbf{0} & \boldsymbol{\Phi}_{\mathbf{r}}^{\mathrm{T}} & \mathbf{0} \\ \mathbf{0} & 4\mathbf{G}^{\mathrm{T}}\mathbf{J}'\mathbf{G} & \boldsymbol{\Phi}_{\mathbf{p}}^{\mathrm{T}} & \boldsymbol{\Phi}_{\mathbf{p}}^{\mathrm{PT}} \\ \boldsymbol{\Phi}_{\mathbf{r}} & \boldsymbol{\Phi}_{\mathbf{p}} & \mathbf{0} & \mathbf{0} \\ \mathbf{0} & \boldsymbol{\Phi}_{\mathbf{p}}^{\mathbf{P}} & \mathbf{0} & \mathbf{0} \end{bmatrix} \begin{bmatrix} \ddot{\mathbf{r}} \\ \ddot{\mathbf{p}} \\ \boldsymbol{\lambda} \\ \boldsymbol{\lambda}^{\mathbf{p}} \end{bmatrix} = \begin{bmatrix} \mathbf{F}^A \\ 2\dot{\mathbf{G}}^{\mathrm{T}}\mathbf{n}'^A + 8\dot{\mathbf{G}}^{\mathrm{T}}\mathbf{J}'\dot{\mathbf{G}}\mathbf{p} \\ \boldsymbol{\gamma} \\ \boldsymbol{\gamma}^{\mathbf{p}} \end{bmatrix}, \tag{3}$$

where, $\boldsymbol{\lambda}$ and $\boldsymbol{\lambda}^{\mathbf{p}}$are the vectors of Lagrange multipliers, and

$$\boldsymbol{\Phi}_{\mathbf{p}}^{\mathbf{p}} = 2\begin{bmatrix} \mathbf{p}_a^{\mathrm{T}} & 0 & \cdots & 0 \\ 0 & \mathbf{p}_b^{\mathrm{T}} & \cdots & 0 \\ \vdots & & & \\ 0 & 0 & \cdots & \mathbf{p}_{L6}^{\mathrm{T}} \end{bmatrix} \tag{4}$$

with

$$\boldsymbol{\gamma}^{\mathbf{p}} = -2\begin{bmatrix} \dot{\mathbf{p}}_a^{\mathrm{T}}\dot{\mathbf{p}}_a \\ \dot{\mathbf{p}}_b^{\mathrm{T}}\dot{\mathbf{p}}_b \\ \\ \dot{\mathbf{p}}_{L6}^{\mathrm{T}}\dot{\mathbf{p}}_{L6} \end{bmatrix}. \tag{5}$$

Here $\boldsymbol{\Phi}_{\mathbf{r}}$, $\boldsymbol{\Phi}_{\mathbf{p}}$ and $\boldsymbol{\gamma}$ are, respectively, the assembled constraint Jacobian and the acceleration equation of the joints. In this paper the 6-TPS platform (6 Spherical joints, 6 Universal joints and 6 Cylindrical joints) is studied. The detailed derivation of the constraint equations for these joints is given in Ref. [12].

3.2. Driven force of the legs

The plant is controlled by adjusting the six actuators when the base platform is disturbed by winds or other unknown excitations. Let $u_i(t)$ be the driven force of the ith leg, in this case

$$u_i(t) = u_i\{l_i(t), \dot{l}_i(t)\} \quad (i = 1, \ldots, 6), \tag{6}$$

where $l_i(t)$ and $\dot{l}_i(t)$ are, respectively, the length and sliding velocity of the ith leg.

For the ith actuator, the general driven force vector acted on the base and stabilized platforms can be partitioned as

$$\begin{bmatrix} \mathbf{F}_{ai} \\ \mathbf{n}'_{ai} \end{bmatrix} = \frac{u(t)_i}{\mathrm{d}_{UiLi}} \begin{bmatrix} \mathbf{d}_{UiLi} \\ 2\mathbf{G}_a^{\mathrm{T}} \tilde{\mathbf{s}}'_{ai} \mathbf{A}_a^{\mathrm{T}} \mathbf{d}_{UiLi} \end{bmatrix},$$
$$\begin{bmatrix} \mathbf{F}_{bi} \\ \mathbf{n}'_{bi} \end{bmatrix} = -\frac{u(t)_i}{\mathrm{d}_{UiLi}} \begin{bmatrix} \mathbf{d}_{UiLi} \\ 2\mathbf{G}_b^{\mathrm{T}} \tilde{\mathbf{s}}'_{bi} \mathbf{A}_b^{\mathrm{T}} \mathbf{d}_{UiLi} \end{bmatrix}, \tag{7}$$

where d_{UiLi} is the length of vector $\mathbf{d}_{UiLi}$. $\mathbf{A}_i$ represents the transformation matrix of the ith rigid body with respect to the global reference frame defined in Eq. (A.6) (see Appendix A). The top operator "$\sim$" gives the skew matrix of a vectors. Thus in Eq. (7), $\tilde{\mathbf{s}}$ is defined as

$$\tilde{\mathbf{s}} = \begin{bmatrix} 0 & -s_z & s_y \\ s_z & 0 & -s_x \\ -s_y & s_x & 0 \end{bmatrix}. \tag{8}$$

3.3. The supporting cable

In the analysis of the plant, the supporting cables are modelled with springs and dampers. Consider the spring-damper model, shown in Fig. 5, which connects point P_i ($i = 1, \ldots, 12$) on the base platform and P_j ($j = 1, \ldots, 12$) on the fixed reference frame (in the radio telescope, P_j is on

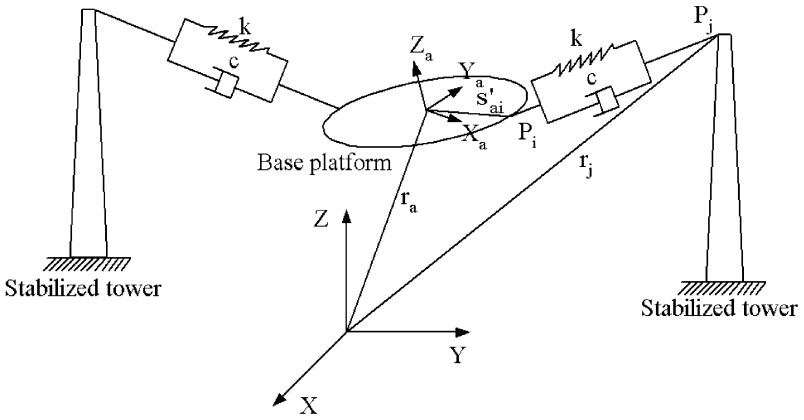

Fig. 5. Spring–damper model of cable.

the stabilized tower or on the ground). The vector from P_i to P_j is

$$\mathbf{d}_{ij} = \mathbf{r}_j - \mathbf{r}_a - \mathbf{A}_a \mathbf{s}'_{ai}. \tag{9}$$

Thus, the square of the length of the cable is given by

$$l_{ij}^2 = \mathbf{d}_{ij}^{\mathrm{T}} \mathbf{d}_{ij} \tag{10}$$

and the time rate of the change of the length is

$$\dot{l}_{ij} = \left(\frac{\mathbf{d}_{ij}}{l_{ij}}\right)^{\mathrm{T}} (\dot{\mathbf{r}}_j - \dot{\mathbf{r}}_a \mathbf{A}_a \tilde{\mathbf{s}}'_{ai} \boldsymbol{\omega}'_a), \tag{11}$$

where $\boldsymbol{\omega}'$ represents the relative angular velocity of the rigid body defined as

$$\boldsymbol{\omega}' = 2\mathbf{G}\dot{\mathbf{p}}. \tag{12}$$

The magnitude of force acting on the base platform by the jth cable, with tension taken as positive, is

$$f_j = k(l_{ij} - l_{ij0}) + c\dot{l}_{ij}, \tag{13}$$

where k is the spring coefficient, c is the damping coefficient, and l_{ij0} is the initial length of the jth cable.

Thus, in term of Euler parameters of the general constrained force acted on the base platform is given by

$$\begin{bmatrix} \mathbf{F}_{aj} \\ \mathbf{n}'_{aj} \end{bmatrix} = \frac{f_j}{l_{ij}} \begin{bmatrix} \mathbf{d}_{ij} \\ 2\mathbf{G}_a^{\mathrm{T}} \tilde{\mathbf{s}}'_{ai} \mathbf{A}_a^{\mathrm{T}} \mathbf{d}_{ij} \end{bmatrix}. \tag{14}$$

The general control force vectors acting on the base platform by the 12 cables are

$$\begin{bmatrix} \mathbf{F}_a \\ \mathbf{n}'_a \end{bmatrix} = \begin{bmatrix} \sum_{i=1}^{12} \mathbf{F}_{aj} \\ \sum_{i=1}^{12} \mathbf{n}'_{aj} \end{bmatrix}. \tag{15}$$

4. The PD control law based on the prediction

4.1. The prediction of the platform

Due to the large inertia of the base platform, the motion of the base platform can be predicted in short time with the current states. Let T be the sample interval in seconds, $\mathbf{x}(k)$ be the value of $\mathbf{x}$ at kT (k is an integer). The position of the base platform $\bar{\mathbf{r}}_a(k+1)$ can be predicted in the next T with

$$\bar{\mathbf{r}}_a(k+1) = \hat{\mathbf{r}}_a(k) + \hat{\mathbf{v}}_a(k)T + 0.5\hat{\mathbf{a}}_a(k)T^2 \tag{16}$$

Here, $\hat{\mathbf{r}}_a(k)$, $\hat{\mathbf{v}}_a(k)$ and $\hat{\mathbf{a}}_a(k)$ are, respectively, the current observed position vector, the velocity vector and acceleration vector of the base platform. So the predicted position $\bar{\mathbf{r}}_{ai}^P(k+1)$ of the upper mounting point of the ith actuator P_{ai} (see Fig. 4) is

$$\bar{\mathbf{r}}_{ai}^P(k+1) = \bar{\mathbf{r}}_a(k+1) + \mathbf{A}_a(k+1)\mathbf{s}'_{ai}. \tag{17}$$

Take the predicted position of the base platform as reference signals, a control for the next T is: adjust the lengths of the legs making the stabilized platform at the ideal position while the base platform at the predicted position. It is illustrated in Fig. 6, where $\bar{l}_i(k+1)$ and $l_i(k)$ are, respectively, the predicted and current length of the ith actuator strut.

As shown in Fig. 4, denote $\bar{\mathbf{r}}_{bi}^P = \bar{\mathbf{r}}_b + \mathbf{A}_b\mathbf{s}'_{bi}$ the ideal position vectors of point P_{ai} of the stabilized platform in the global reference frame. The predicted lengths of the legs can be expressed as

$$\bar{l}_i(k+1) = \|\bar{\mathbf{r}}_{ai}^P(k+1) - \bar{\mathbf{r}}_{bi}^P(k+1)\| \quad (i = 1, \ldots, 6). \tag{18}$$

By the same method of obtaining Eq. (11), the sliding velocities of the ith leg are

$$\dot{\bar{l}}_i(k+1) = \frac{(\bar{\mathbf{r}}_{ai}^P(k+1) - \bar{\mathbf{r}}_{bi}^P(k+1))^{\mathrm{T}}}{\bar{l}_i(k+1)}(\hat{\mathbf{v}}_a(k) + \dot{\mathbf{A}}_a\mathbf{s}'_{ai} - \bar{\mathbf{v}}_b(k) - \dot{\mathbf{A}}_b s'_{bi}), \tag{19}$$

where $\bar{\mathbf{v}}_b$ is the ideal velocity of the stabilized platform.

The position vector of the base platform can be sampled:

$$\mathbf{r}_a(k),\ \mathbf{r}_a(k-1),\ \mathbf{r}_a(k-2), \ldots\ . \tag{20}$$

As the three-dimensional velocities and the accelerations of the base platform are difficult to measure in such low frequency (about 0.2 Hz), only the position responses of the base platform are directly measured and the velocities and accelerations are estimated by the finite difference method. For smoothing the velocity, the following equations can be used for the velocity:

$$\hat{\mathbf{v}}_a(k) = \frac{1.5\mathbf{r}_a(k) + 0.5\mathbf{r}_a(k-2) - 2\mathbf{r}_a(k-1)}{T} \tag{21}$$

and the accelerations can be obtained as

$$\hat{\mathbf{a}}_a(k) = \frac{\hat{\mathbf{v}}_a(k) - \hat{\mathbf{v}}_a(k-1)}{T}. \tag{22}$$

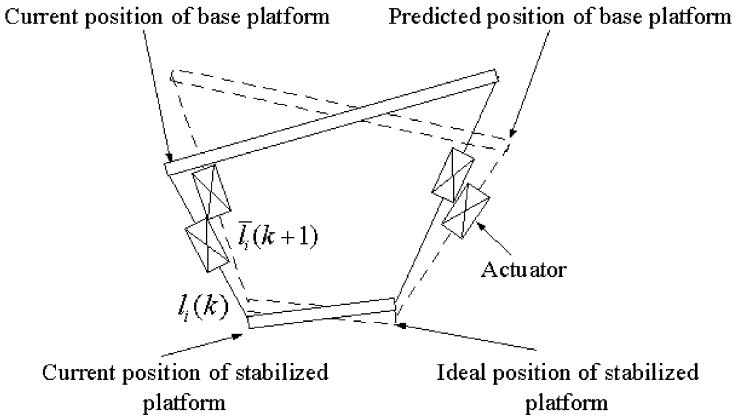

Fig. 6. Predicted lengths of the actuators.

4.2. The PD control law

Since the objective of this application is to stabilize the stabilized platform, we assume it almost still in the global frame. Thus, the control laws not considering dynamic coupling of the two platforms can be used to see whether or not could the stabilized platform be controlled. Based on above prediction of the two platforms, a PD control law is proposed to stabilize the lower platform. The errors between the predicted and the present lengths and sliding velocities of the legs are used to determine the required force of the six actuators. The control law of the ith leg can be written in the following form:

$$u_i(k+1) = -(K_p)_i(\bar{l}_i(k+1) - l_i(k))\bar{i}_i(k+1), \quad i = 1, 2, \ldots, 6, \tag{23}$$

where $(K_p)_i$ and $(K_v)_i$ are, respectively, the position and velocity gains.

5. Simulation results

In this section, simulation results for the plant are computed via the model described in the previous sections. The dimensions of the plant are shown in Fig. 7. The system includes: base platform, the stabilized platform and the six actuators. The base platform is supported by 12 springs, including 8 suspension springs and 4 stabilized springs (see Fig. 2). The parameters of the Gough–Stewart platform are given in Appendix B.

The Adaptive Adams methods with Runge–Kutta Starters [13] and the generalized co-ordinate partitioning approach [12] are used to solve Eq. (3). The algorithms are implemented with the object-oriented C++ language.

In the simulations, the assumed values of position and velocity gains of the Control Law (23) are (arrived at by trail and error), respectively, $(K_p)_i = 20,0000$ and $(K_v)_i = 24,500$ for $i = 1, 2, \ldots, 6$. The spring coefficient of the springs is 20,000 N/m and the damping ratio $\xi = 0.05$. The selection of the parameters of the springs is to insure that the main frequency of the plant is about 0.2 Hz. For the simulation model the stable control-updating period is 0.1 s and control lag is 0.02 s.

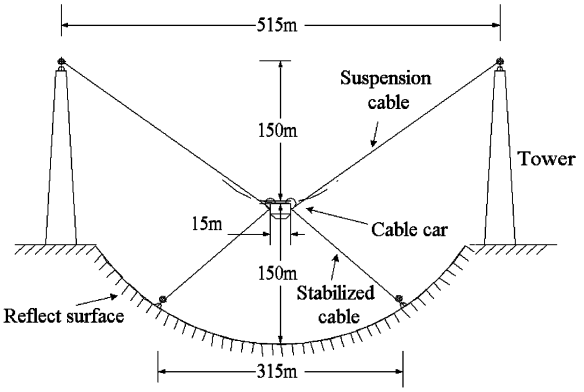

Fig. 7. Dimensions of the plant.

5.1. The simulation of wind load

According to the past records, the maximum horizontal wind velocity in the area where the radio telescope will be set up is 8.2 m/s. The wind load on the cable car is simplified as concentrated forces applied at the center of the base platform. As the area of cable car is 15 m × 8 m, the maximum horizontal force acting on the cable car is about 10,000 N. The area of the 12 cables is about (300 m × 8 + 150 × 4) × 0.04 m (assume the diameter of cables is 0.04 m), the maximum wind load on these cables is about 10,000 N. Half the load is equivalent on the cable car. So the equivalent wind load on the cable car is about 15,000 N. Three random samples are generated in three directions. Every sample includes a mean part of 15,000 N and a pulsating part of 1000 N. One of the force samples is shown in Fig. 8.

The responses of the centers of mass of the base platform and the stabilized platform in X and Z directions and the rotation of the platforms around the X-axis are compared in Fig. 9.

The time histories of stroking forces and the sliding velocity of a typical leg are depicted, respectively, in Figs. 10 and 11.

The root-mean-square deviation in X, Y and Z direction and around X-, Y- and Z-axis of the base platform and the stabilized platform are compared in Table 1. It implies that the amplitude of the vibration could be reduced more than 15 times by the PD control law.

According to the above simulating results, the request of the sliding velocity is 1 m/s, the maximum elongation of the legs is 1.5 m and the maximum and minimum lengths of each leg are, respectively, 8.6 and 7.1 m.

5.2. The dynamic responses of step input

As the transfer function or frequency response data of the system is difficult to obtained, in order to study the effect of the dynamic coupling between the two platforms, the responses of the two platforms on a step position input to the stabilized platform are simulated.

The dynamic responses of the two platforms under a step position change of 0.5 m on the stabilized platform in X and Z directions in the global reference frame from zero initial velocity of both platforms are shown, respectively, in Figs. 12 and 13. From the figures, one can see that the

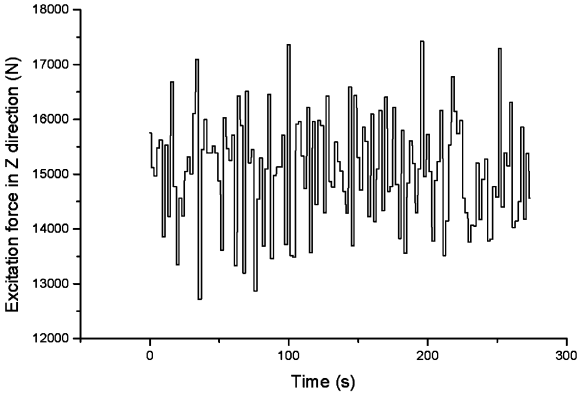

Fig. 8. Sample of wind loads.

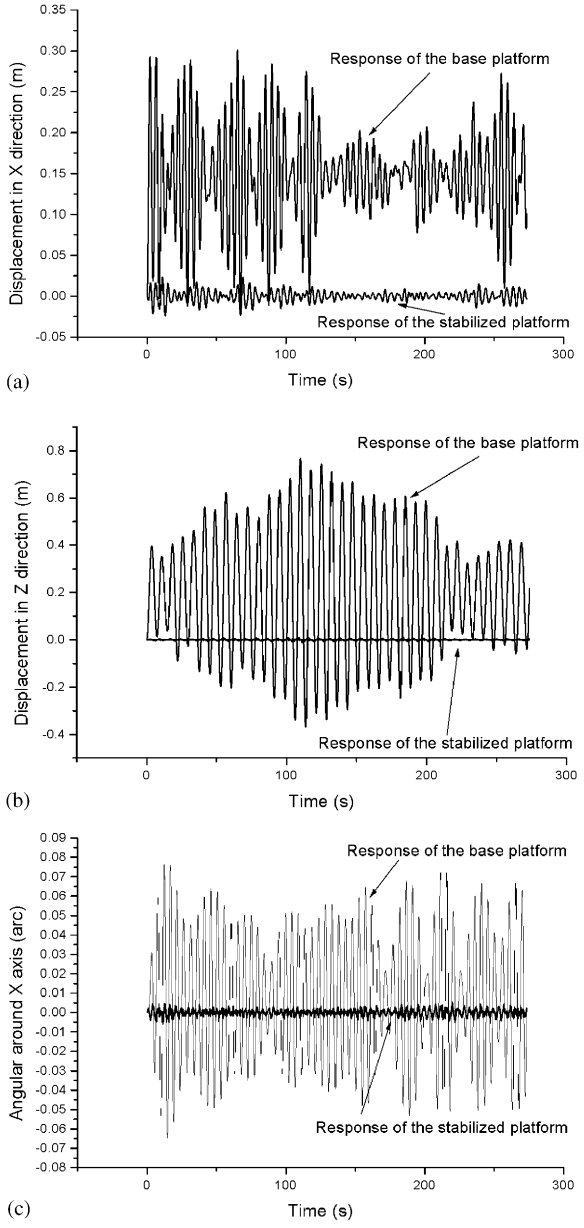

Fig. 9. Time histories of the responses of the two platform (with PD control): (a) displacement in X direction, (b) displacement in Z direction, (c) the angular responses around X-axis.

reaction forces caused by the motion of the stabilized platform leads to perturbation on the base platform. The time history of stroking force of a typical leg with respect to a step position input of 0.5 m on the stabilized platform in X direction is depicted on Fig. 14. It shows that the stroking force of the leg is convergent after a step load is put on the system.

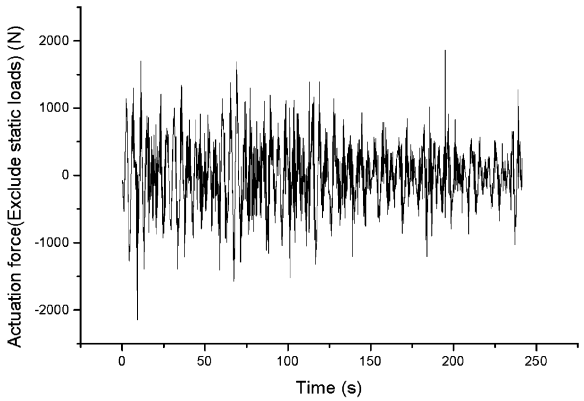

Fig. 10. Variation of the actuation forces.

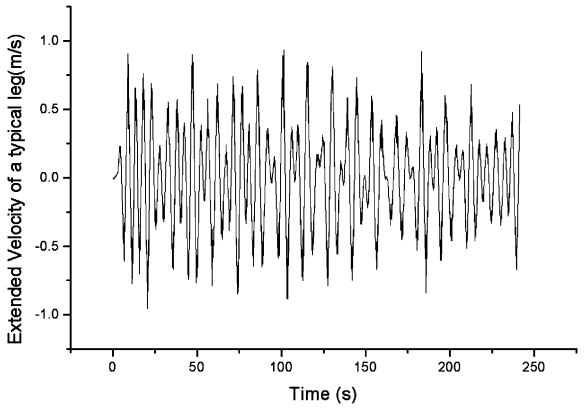

Fig. 11. Elongation velocity of the typical leg.

Table 1
Response of root-mean-square deviation

	X (m)	Y (m)	Z (m)	θ_x (deg)	θ_y (deg)	θ_z (deg)
Base platform	0.094	0.122	0.279	1.68	1.32	0.004
Stabilized platform	0.0064	0.0067	0.0035	0.09	0.08	0.006

6. Conclusions

This paper studies the feasibility of using the Gough–Stewart parallel mechanism to stabilize a platform on a vibrating base platform. The stabilization problem is equivalent to a dynamics and control problem of rigid multi-body system. The PD control law is proposed for the six actuators

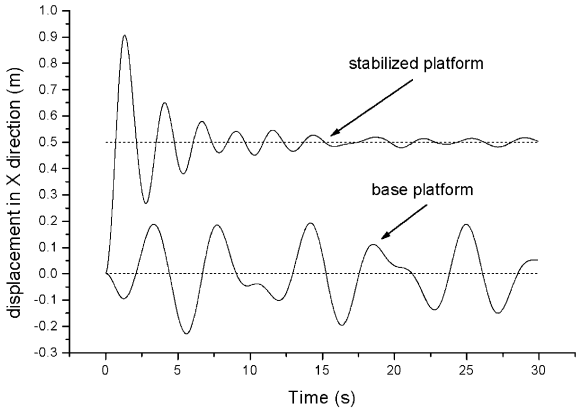

Fig. 12. Step responses in X direction.

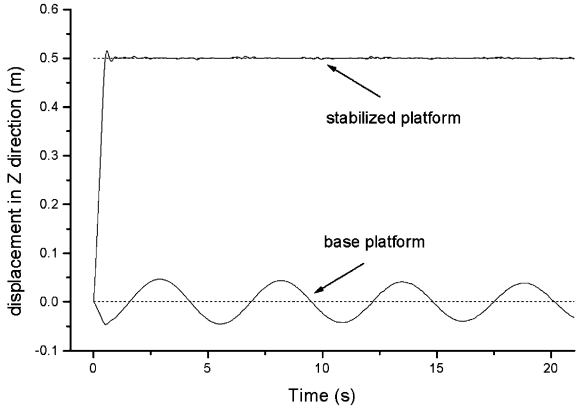

Fig. 13. Step responses in Z direction.

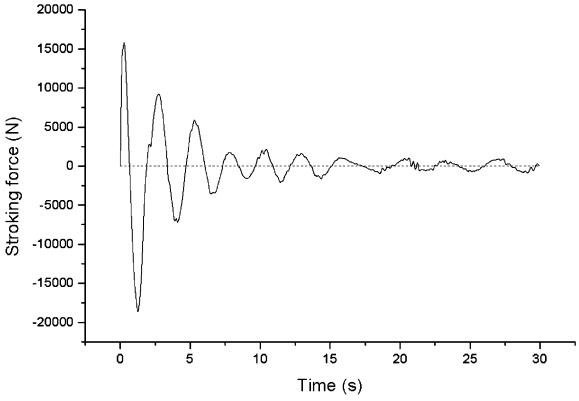

Fig. 14. The stroking force of a typical leg with respect to a step input of 0.5 m in stabilized platform in X direction.

of the system, in which the predicted inertial motion of the base platform is used as the reference input for the control problem. The finite difference method is used to estimate the velocity and acceleration of the base platform from the measured displacement. The simulations of the system show that the Gough–Stewart platform, with the proposed control law, is effective for vibration stabilization provided the control updating frequency is high enough.

The prediction and PD control law suggested in Section 4 can be used in real-time control. In practical applications, the rigid body position and orientation of the base and stabilized platforms can be determined by measuring the co-ordinates of three points with optical methods. In our present experiment on a model system (1:10), the position of base platform is measured with three Laser Automatic Total Stations (TPS1100), whose positioning accuracy is $\leqslant 1$ mm (for static measure), and $\leqslant 3$ mm (for tracking).

Acknowledgements

This work was supported by the research fund for large radio telescope, Chinese National Astronomical Observatories, the fundamental research fund (No. JC1999031) of Tsinghua University and NNSF (Project No. 10172049).

Appendix A. The generalized co-ordinate of Euler parameters

Euler parameters [12] are used as the orientation parameters of a body with the normalization relationship as the algebraic constraint. The base point co-ordinates of the centroidal body-fixed reference frame of ith body in the global frame are denoted by

$$\mathbf{r}_i = (x_i \quad y_i \quad z_i)^{\mathrm{T}}. \tag{A.1}$$

The Euler parameters for the ith body are denoted by

$$\mathbf{p}_i = (e_i^0 \quad e_i^1 \quad e_i^2 \quad e_i^3)^{\mathrm{T}}. \tag{A.2}$$

The normalization condition is

$$\mathbf{\Phi}_i^{\mathbf{p}} = \mathbf{p}_i^{\mathrm{T}}\mathbf{p}_i - 1 = 0. \tag{A.3}$$

Two 3×4 matrix $\mathbf{E}_i$ and $\mathbf{G}_i$ is defined as

$$\mathbf{E}_i = \begin{bmatrix} -e_i^1 & e_i^0 & -e_i^3 & e_i^2 \\ -e_i^2 & e_i^3 & e_i^0 & -e_i^1 \\ -e_i^3 & -e_i^2 & e_i^1 & e_i^0 \end{bmatrix}, \tag{A.4}$$

$$\mathbf{G}_i = \begin{bmatrix} -e_i^1 & e_i^0 & e_i^3 & -e_i^2 \\ -e_i^2 & -e_i^3 & e_i^0 & e_i^1 \\ -e_i^3 & e_i^2 & -e_i^1 & e_i^0 \end{bmatrix}. \tag{A.5}$$

The transformation matrix

$$\mathbf{A} = \mathbf{E}\mathbf{G}^{\mathrm{T}}. \tag{A.6}$$

Table 2
Inertia parameters of the plant

	Mass (kg)	Inertia $J_x = J_y$(kg m^2)	Inertia J_z (kg m^2)
Base platform	46,300	266,688	533,376
Stabilized platform	4600	2944	5888
Upper legs	500×6	625×6	2.5×6
Low legs	20×6	5×6	0.5×6

Table 3
Initial positions of the platforms

	X (m)	Y (m)	Z (m)	e^0	e^1	e^2	e^3
Base platform	0	0	0	1	0	0	0
Stabilized platform	0	0	−0.702	1	0	0	0

Appendix B. The parameters of the Gough–Stewart platform

The details of the Stewart parallel mechanism used in this application are given as follow:
Base platform (in the base platform frame):

$$P_{ai} = \begin{bmatrix} 4.9\cos(2(i-1)\pi/3 \pm \pi/12) & 4.9\sin(2(i-1)\pi/3 \pm \pi/12) & 0 \end{bmatrix}^{\mathrm{T}}, \quad i = 1, 2, 3.$$

Stabilized platform (in the stabilized frame):

$$P_{bi} = \begin{bmatrix} 1.8\cos(\pm i\pi/3) & 1.8\sin(\pm i\pi/3) & 0 \end{bmatrix}^{\mathrm{T}}, \quad i = 1, 2, 3.$$

The upper and lower mounting point P_{ai} and P_{bi} in their local frame $X'_{Ui}Y'_{Ui}Z'_{Ui}$ and $X'_{Li}Y'_{Li}Z'_{Li}$ are (see Fig. 4)

$$P^i_{ai} = \begin{bmatrix} 0 & 0 & 2 \end{bmatrix}^{\mathrm{T}}, \quad i = 1, 2, \ldots, 6$$

and

$$P^i_{bi} = \begin{bmatrix} 0 & 0 & 0.2 \end{bmatrix}^{\mathrm{T}}, \quad i = 1, 2, \ldots, 6.$$

The inertia parameters of the system and initial positions of the platforms are listed, respectively, in Tables 2 and 3. (The initial velocities and accelerations of the two platforms are zero.)

References

[1] D. Stewart, Aplatform with six degrees of freedom, Proceedings of the Institution of Mechanical Engineers 180 (5) (1965) 371–386.

[2] Li Hui, China hopes to move FAST on largest telescope, Science 281(5378) (1998) 771–773.
[3] Hong Wang, Yanlin Guo, Gexue Ren, Yingjie Lu and Guibin Lin, Experimental Study and Theoretical Analysis of the Structure for Supporting the Deed Cabin of the FAST, Journal of Building Structures (in Chinese), 23 (3) (2002) 63–68.
[4] G.X. Ren, Q.H. Lu, Z. Zhou, On the cable car feed support configuration for FAST, Astrophysics and Aerospace Science 278 (2001) 243–247.
[5] E.F. Fichter, Stewart platform-based manipulator: general theory and practical construction, International Journal of Robotics Research 5 (2) (1986) 157–182.
[6] G. Lebret, K. Liu, F.L. Lewis, Dynamic analysis and control of a Stewart platform manipulator, Journal of Robotic Systems 10 (5) (1993) 629–655.
[7] K. Liu, F. Lewis, G. Lebret, D. Taylor, The singularities and dynamics of a Stewart platform manipulator, Journal of Intelligent and Robotic Systems 8 (3) (1993) 287–308.
[8] Z. Geng, L.S. Haynes, On the dynamic model and kinematic analysis of a class of Stewart platforms, Robotics and Autonomous Systems 9 (4) (1992) 237–254.
[9] B. Dasgupta, T.S. Mruthyunjaya, Closed-form dynamic equations of the general Stewart platform through the Newton–Euler approach, Mechanism and Machine Theory 33 (7) (1998) 993–1012.
[10] Z. Geng, L.S. Haynes, Six degree-of-freedom active vibration isolation using Stewart platform manipulator, Journal of Robotics Systems 10 (5) (1993) 725–744.
[11] R.G. Cobb, J.M. Sullivan, A. Das, L. Porter, Vibration isolation and suppression system for precision payloads in space, Smart Material and Structures 8 (1999) 791–797.
[12] E.J. Haug, Computer-Aided Kinematics and Dynamics of Mechanical Systems, Vol. 1: Basic Methods, Allyn & Bacon, Boston, 1990.
[13] C.W. Gear, Runge–Kutta starters for multistep method, ACM Transactions on Mathematical Software 6 (3) (1980) 263–279.